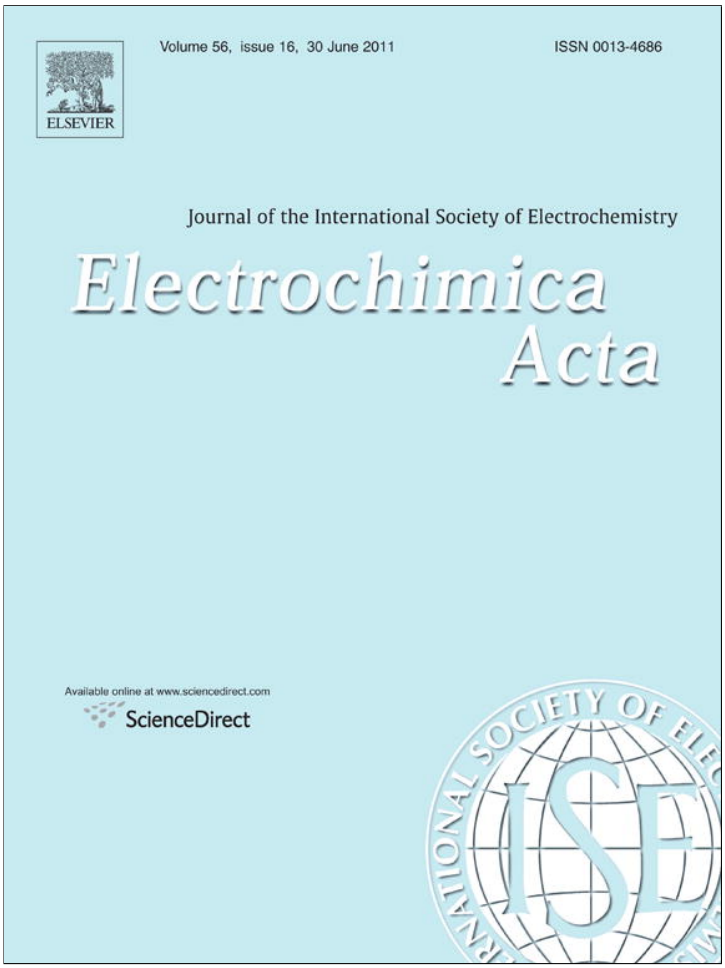

Electrochimica Acta 56 (2011) 5673–5678

Contents lists available at ScienceDirect

Electrochimica Acta

journal homepage: www.elsevier.com/locate/electacta

Electrochemical performance of single crystalline spinel $LiMn_2O_4$ nanowires in an aqueous $LiNO_3$ solution

Mingshu Zhao*, Xiaoping Song, Fei Wang, Weimin Dai, Xuegang Lu

MOE Key Laboratory for Nonequilibrium Synthesis and Modulation of Condensed Matter, School of Science, Xi'an Jiaotong University, 710049 Xi'an, China

ARTICLE INFO

Article history:
Received 14 February 2011
Received in revised form 2 April 2011
Accepted 9 April 2011
Available online 22 April 2011

Keywords:
Electrochemical properties
Aqueous rechargeable lithium battery
Spinel $LiMn_2O_4$ nanowire
Single crystalline

ABSTRACT

Single crystalline cubic spinel $LiMn_2O_4$ nanowires were synthesized by hydrothermal method and the precursor calcinations. The phase structures and morphologies were characterized by X-ray diffraction (XRD), field emission scanning electron microscopy (FESEM), and high-resolution transmission electron microscopy (HRTEM). Galvanostatic charging/discharging cycles of as-prepared $LiMn_2O_4$ nanowires were performed in an aqueous $LiNO_3$ solution. The initial discharge capacity of $LiMn_2O_4$ nanowires was 110 mAh g^{-1}, and the discharge capacity was still above 100 mAh g^{-1} after 56 cycles at 10C-rate, and then 72 mAh g^{-1} was registered after 130 cycles. This is the first report of a successful use of single crystalline spinel $LiMn_2O_4$ nanowire as cathode material for the aqueous rechargeable lithium battery (ARLB).

1. Introduction

The spinel $LiMn_2O_4$ material is considered as one of promising cathode materials for rechargeable lithium batteries (LIB) due to its low cost, fast charging–discharging reactions, high coulombic efficiency and no toxicity [1–3]. However, its disadvantage is poor cycling behavior caused by Jahn-Teller distortion and manganese dissolution into organic electrolyte [4–6]. How to improve its discharge specific capacity during cycles is very pronounced. Researchers attempt to improve its cycle stability using various approaches, such as replacement of manganese with other transition metal element [7–12], surface coating [13,14] and etc. [15–17]. Although the organic electrolyte has advantages of wide electrochemical windows, it is easily flammable, low conductivity and high cost. Whereas, aqueous electrolyte solution has features of safety, high conductivity and low cost.

Dahn et al. first reported ARLB assembling with $LiMn_2O_4$ and VO_2 in 5 M $LiNO_3$ aqueous electrolyte [18–20]. Subsequently, others reported ARLBs using $LiCr_{0.15}Mn_{1.85}O_4$ [10,21], $LiCoO_2$ [22], $LiMn_2O_4$ [23–26], $LiFePO_4$ [27,28], LiV_3O_8 [29] or V_2O_5 [30,31] as electrode materials in $LiNO_3$ [18–27,29–31], Li_2SO_4 [28,32,33], or LiOH [34] aqueous solution.

Recently, nanostructure materials, including three-dimensional (3-D) nanostructure (nano flower-shaped, nano coral-like, hollow, meso-porous, core-shell, multideck-cage), two-dimensional (2-D) nanostructure (nanobelts, nanosheets, nanoplatelets, nanospindles), one-dimensional (1-D) nanostructure (nanorods, nanotubes, porous nanotubes, nanowires), and zero-dimensional (0-D) (nanoparticles), have been widely investigated to improve the cycle performance of LIB. Among the above nanostructure, a single crystalline nanowire is the most attractive morphology which has been confirmed in ref. [35–37]. Moreover, nanowire has the potential not only to increase the lithium-ion filled ratio but also to solve the safety problem [35]. Up to now, few papers of $LiMn_2O_4$ single crystalline nanowire or nanorod with cubic structure are reported [38–42].

Herein we reported the electrochemical performance of $LiMn_2O_4$ single crystalline nanowires used as cathode materials for ARLB. We used cyclic galvanostatic charging/discharging experiments in three-electrode cells to evaluate the electrochemical behaviors. To our best knowledge, it is the first report of $LiMn_2O_4$ single crystalline nanowires used in ARLB.

2. Experimental

2.1. $LiMn_2O_4$ preparation and characterization

The fine $LiMn_2O_4$ single crystalline nanowires were prepared by hydrothermal method and calcinations process. The strategic synthesis process was according to the ref. [35]. However, some details were different as follows. Given amount of NaOH (Analytical regent 96%, Tianjin Hengxing Chemical Preparation Co., Ltd. Product) aqueous solution and Mn_3O_4 powders (Analytical reagent 99.5%, Sinopharm Chemical Reagent Co., Ltd. Product) with a stoi-

* Corresponding author. Tel.: +86 029 82663034; fax: +86 029 82667872.
E-mail address: zhaomshu@mail.xjtu.edu.cn (M. Zhao).

0013-4686/$ – see front matter © 2011 Elsevier Ltd. All rights reserved.
doi:10.1016/j.electacta.2011.04.025

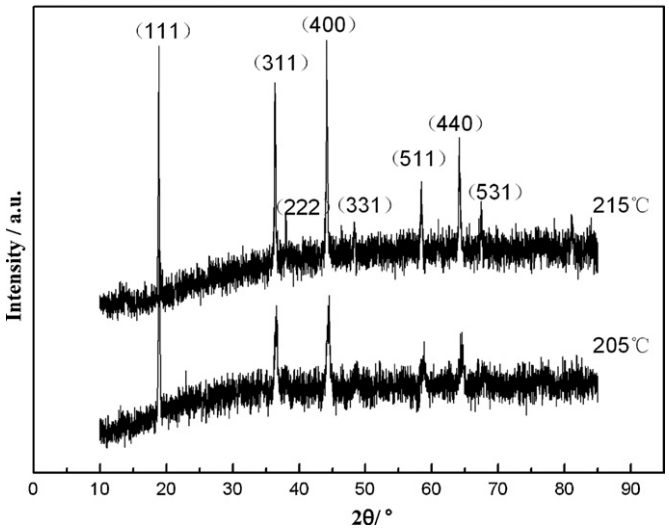

Fig. 1. XRD patterns of $LiMn_2O_4$ nanowires prepared at different hydrothermal temperature of 205 °C or 215 °C.

chiometric molar ratio of 1.32:3 were mixed well in a 50 ml beaker under ultra-sonic for 1 h, and the turbid suspension was transferred to a Telflon-lined stainless steel autoclave, and then heated in an oven at 215 °C (or 205 °C) for 4 d. The precursor was obtained after centrifugation and vacuum dried at 25 °C for 1 d. The obtained precursor, $LiNO_3$ (Analytical reagent, Shanghai Hengxin Chemical Reagent Co., Ltd. Product), and $LiCl{\cdot}H_2O$(Analytical reagent 97%, Shantou Chemical Co., Ltd. Product) were mixed in a mortar and well ground for about 1 h, and then were calcined in air at 500 °C and 800 °C respectively, for 3 h and 1 h. After the first heating process, the sample was washed repeatedly using deionized water for removing sodium ion, chlorion, and nitrate ion. $LiMn_2O_4$ nanowires were obtained after cooled to ambient followed by the second calcinations.

The crystal structure of as-prepared materials was characterized by XRD using Bruker D8-Advanced diffractometer with Cu Ka radiation. The morphology was observed by FESEM and HRTEM with JSM-7000F and JEOL-2100, respectively.

2.2. Electrochemical setup and testing

The ARLB was assembled with working electrode (WE), counter electrode (CE), and reference electrode (RE) in 5 M $LiNO_3$ solution in a 200 ml beaker, which was used for the electrochemical testing. The WE was a composite mixture containing $LiMn_2O_4$ nanowires, acetylene black, and PVDF in NMP solution ratio with 80:10:10 (w/w/w). The mixtures were coated homogeneously on the nickel mesh. The CE active material was LiV_3O_8. The RE was a saturated calomel electrode (SCE). Galvanostatic charging/discharging experiments were performed at 25 °C using software-controled Arbin BT-2000 instrument and the cell potential window was within 0.45–1.2 V.

3. Results and discussion

3.1. Nanowire characterization

The XRD patterns of as-prepared $LiMn_2O_4$ nanowire materials are shown in Fig. 1. The diffractions occurred at $2\theta = 18.61°$, 36.08°, 37.75°, 43.87°, 48.04°, 58.05°, 63.78°and 67.08° correspond to the characteristic diffractions of a pure spinel $LiMn_2O_4$ phase (PDF number 35-0782). As can be seen, when the hydrothermal temperature is increased from 205 °C to 215 °C, the diffraction intensities of the spinels are also increased, and results suggested that the crystallinity of $LiMn_2O_4$ nanowires increase with increasing hydrothermal temperature.

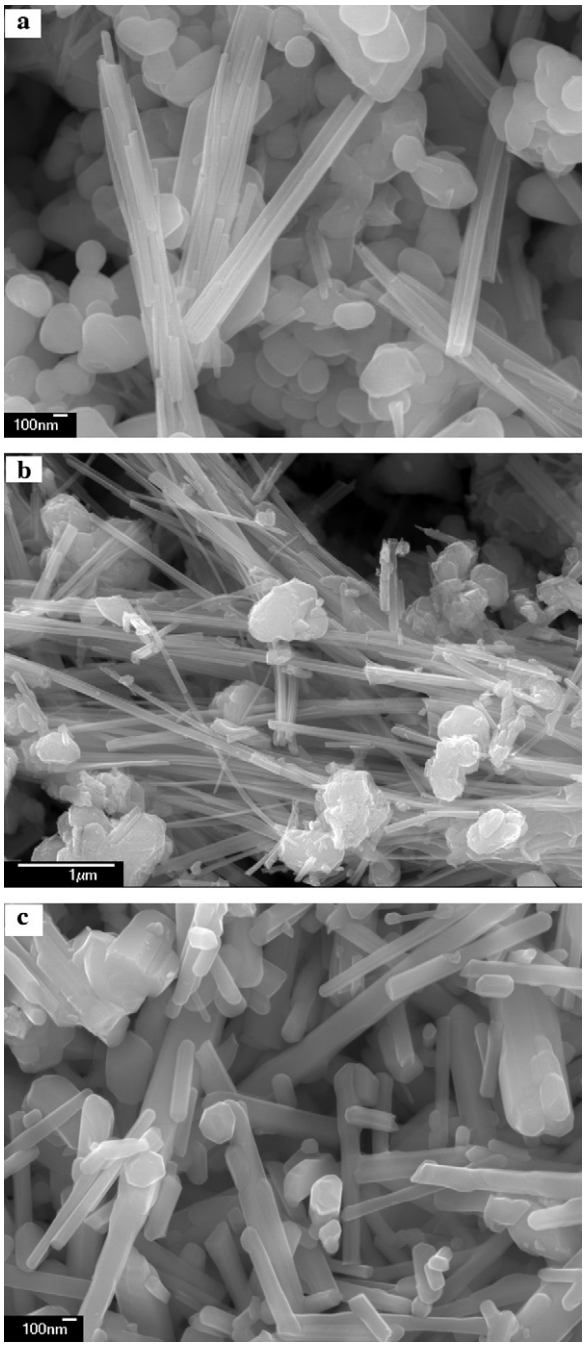

Fig. 2. FESEM images of (a) 205 °C precursor, (b) intermediate calcined at 500 °C and (c) final product calcined at 800 °C.

FESEM images of the $LiMn_2O_4$ nanowires materials are represented in Figs. 2 and 3. When the hydrothermal temperature was 205 °C, the precursor materials express two patterns composed of nanowires and particle plates (Fig. 2a). With the growth continuing after 500 °C calcined, the nanowires are well parallel and particle plates agglomerate, which are distributed on the nanowires (Fig. 2b). Upon further growth calcined at 800 °C, they develop into nanorods (Fig. 2c). Whereas the hydrothermal temperature is 215 °C, whether the precursor or calcined intermediate, and final products, their morphology are all nanowires (Fig. 3a–c). It can be seen from Figs. 2a and 3a that the grain crystallinity increases

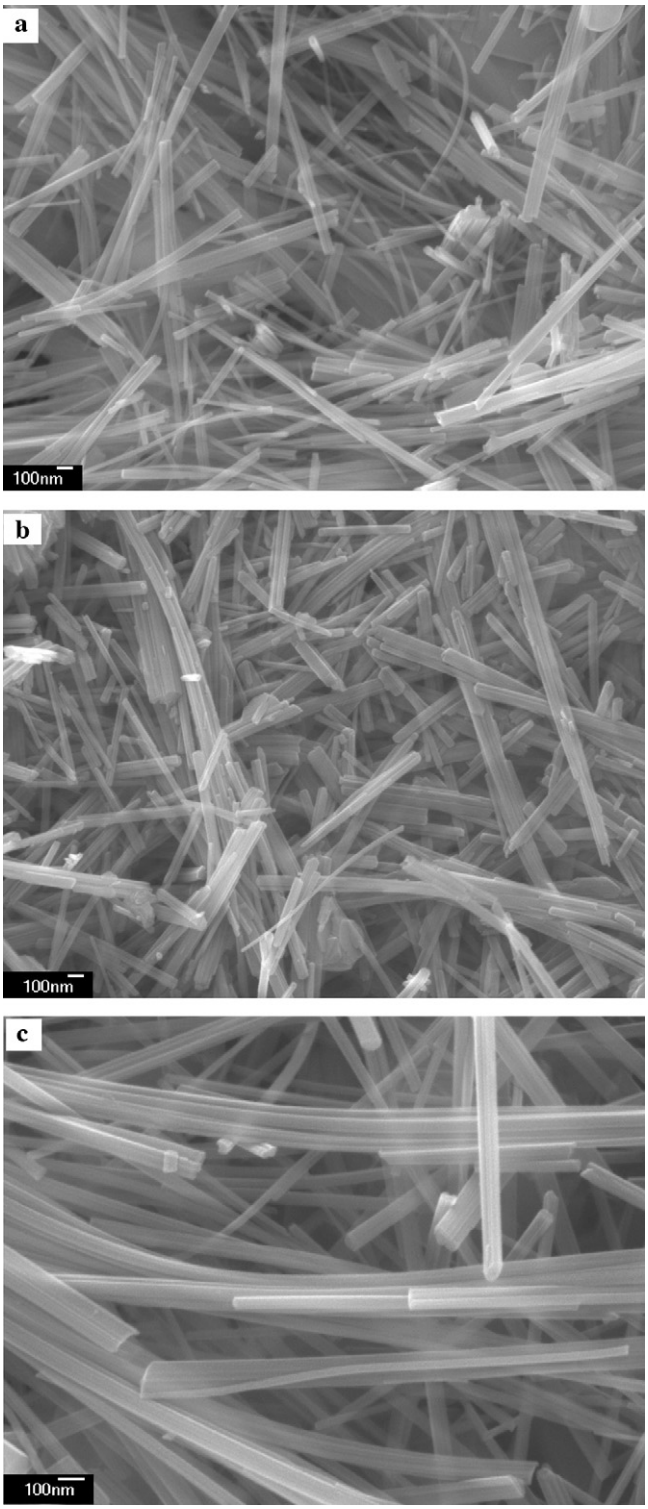

Fig. 3. FESEM images of (a) 215 °C precursor, (b) intermediate calcined at 500 °C and (c) final product calcined at 800 °C.

with increasing hydrothermal temperature, which is in agreement with the XRD results. Moreover, the morphology of the $LiMn_2O_4$ materials is affected by various hydrothermal temperatures.

Fig. 4a and b display TEM images of $LiMn_2O_4$ nanowires. Fig. 4c presents its electron diffraction pattern and Fig. 4d shows its HRTEM images. The results state that single crystalline $LiMn_2O_4$ nanowires, at 215 °C of hydrothermal temperature, is with a diameter of around 80 nm and length up to micrometers can be obtained.

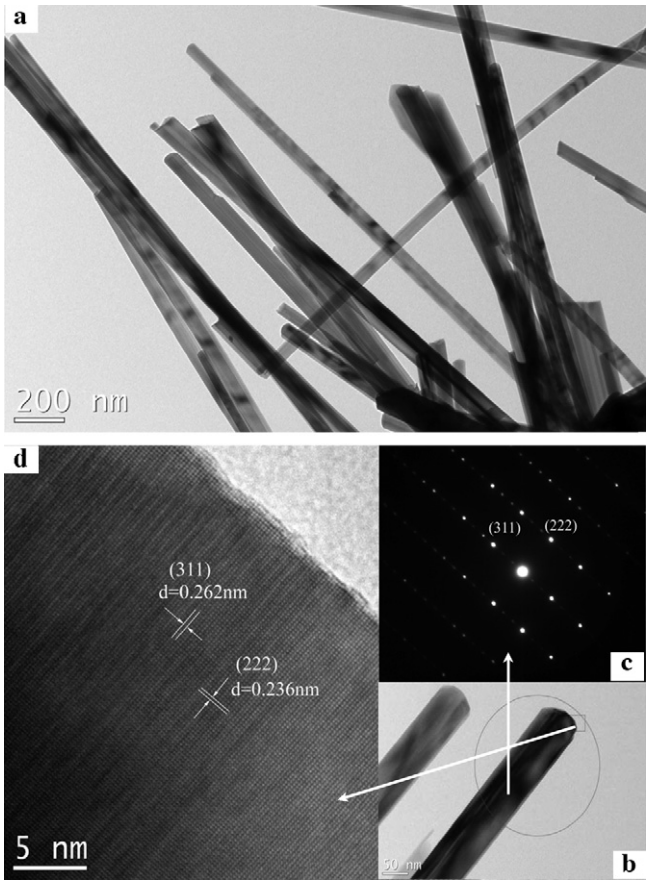

Fig. 4. (a and b) TEM images of $LiMn_2O_4$ nanowires synthesized at hydrothermal temperatures of 215 °C. (c) Electron diffraction pattern and (d) HRTEM image of the selected area.

The spacing of lattice fringes along the wire direction is 0.236 nm, which corresponds to {2 2 2} plane of spinel $LiMn_2O_4$. The in situ electron diffraction pattern can be well indexed such as (3 1 1) and (2 2 2). Accordingly, the clear lattice fringes confirm that the nanowires are single crystalline and the preferential growth direction is [2 2 2].

3.2. Electrochemical performance

Fig. 5a presents charge–discharge curves of LiV_3O_8//$LiMn_2O_4$ (nanowires) ARLBs within the cell potential limits 0.45–1.2 V at 0.2C. It displays that the ARLB potential changes gradually during the charge–discharge process. For the first charing–discharging cycle, we can distinguish the two discharge plateaus, one at the mean potential of 0.95 V and the other at the mean potential of 0.85 V for $LiMn_2O_4$ nanowires (215 °C) (dashed line in Fig. 5a). Seemly for those of $LiMn_2O_4$ nanowires (205 °C) can be observed at about 0.9 V and 0.8 V or so (solid line in Fig. 5a). This is consistent with the behavior of spinel-like $LiMn_2O_4$ materials in organic electrolytes [5,6]. In Fig. 5, the cell open circuit potentials of the two samples are different due to the polarization resistance. And the cell open circuit potential could be used to estimate the charged state, which is not a criterion to measure the cell potential during the charge–discharge process. Moreover, the coulombic efficiency of the two samples is different at 0.2C in Fig. 5 because the charge transfer reaction between the electrode active material and aqueous electrolyte interface is different. And this charge transfer reaction rate is strongly related to the capability of the charge–discharge reaction and then the coulombic efficiency of these two samples is different.

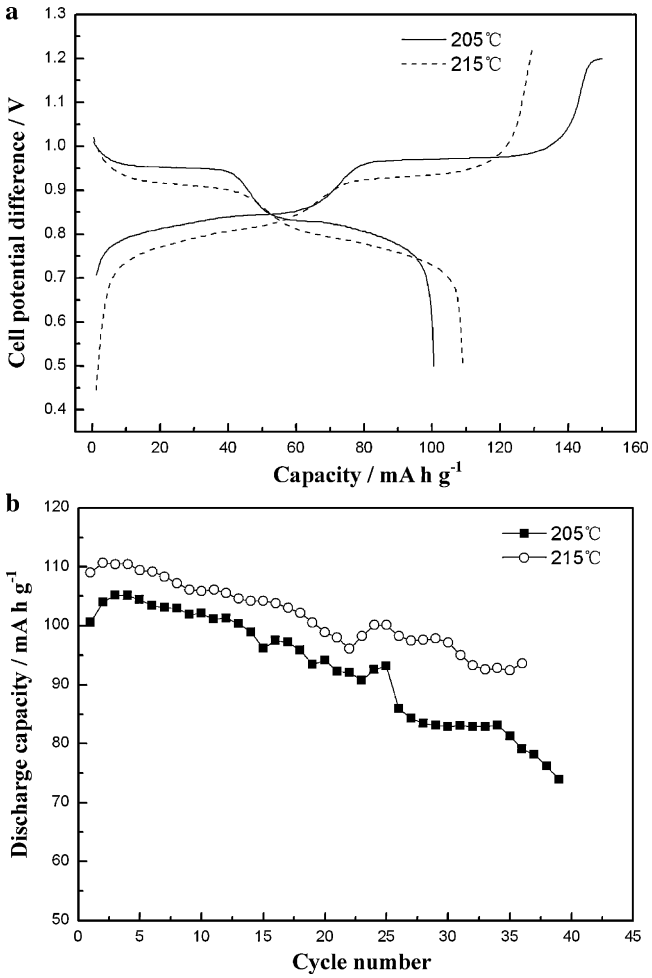

Fig. 5. Electrochemical performance of LiV_3O_8//$LiMn_2O_4$ (nanowires synthesized at different hydrothermal temperatures of 205 °C or 215 °C) for ARLBs (a) 1st charge–discharge curves at 0.2C. (b) Cycle performance at 0.2C.

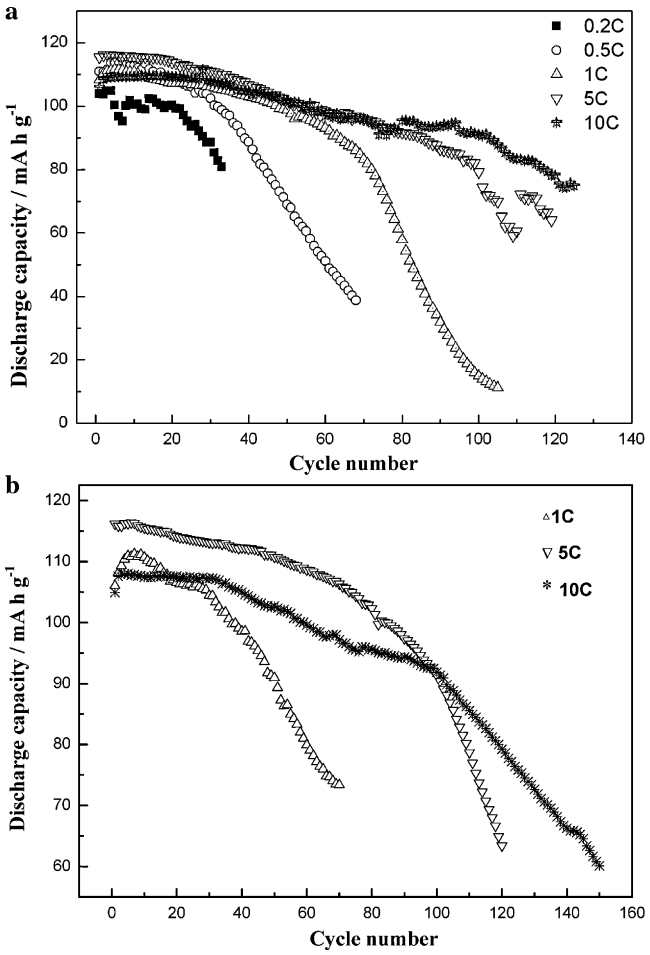

Fig. 6. (a) Cycling behaviors of LiV_3O_8//$LiMn_2O_4$ (nanowires synthesized at hydrothermal temperatures of 215 °C) at different discharge rate of 0.2C, 0.5C, 1C, 5C and 10C. (b) Cycling behaviors of LiV_3O_8//$LiMn_2O_4$ (nanowires synthesized at hydrothermal temperatures of 205 °C) at different discharge rate of 1C, 5C and 10C.

For the sake of comparison, discharging capacities of this material in the first 36 cycles at 0.2C, which was synthesized at different hydrothermal temperature of 215 °C or 205 °C, are illustrated in Fig. 5b. In comparison to the cycling behavior of $LiMn_2O_4$ nanowires (215 °C) in ARLB, $LiMn_2O_4$ nanowires (205 °C) display here lower initial discharging capacity and its cyclability is not much better (full squares in Fig. 5b). However, the initial discharge capacity for $LiMn_2O_4$ nanowires synthesized at hydrothermal temperature of 215 °C is 110 mAh g^{-1} and the capacity also remains 95 mAh g^{-1} after 36 cycles (hollow circles in Fig. 5b). The results also indicate that the single crystalline $LiMn_2O_4$ nanowire at higher hydrothermal temperature has better electrochemical performance.

In order to investigate rate performance of $LiMn_2O_4$ nanowires ARLB at various discharging rates, Fig. 6a displays cycling stability of LiV_3O_8//$LiMn_2O_4$ nanowires (which was prepared at hydrothermal temperature of 215 °C) ARLB at 0.2C, 0.5C, 1C, 5C and 10C. The initial discharge capacity of the ARLB is 110 mAh g^{-1}, and the retained discharge capacity is still above 100 mAh g^{-1} after 56 cycles at 10 C-rate, and then 72 mAh g^{-1} is registered after 130 cycles, which indicates the better cyclability in aqueous $LiNO_3$ solution at higher discharge rate. To obtain excellent battery performance, the surface of the active materials is very important [35]. The surface of as-prepared single crystalline nanowires is a very pure and clean surface based on the facet plane of {2 2 2}. So we think that the nanowires are suitable for the higher power performance of ARLB. However, the influence of the discharging rate on the specific capacity is quite different from that of the organic LIB [42] or the other ARLB [21]. Fig. 6b illustrates LiV_3O_8//$LiMn_2O_4$ nanowires (which was prepared at hydrothermal temperature of 205 °C) ARLB at 1C, 5C and 10C. It can be seen that the cycling stability of this $LiMn_2O_4$ nanowires material is not better than that of the other sample prepared at hydrothermal temperature of 215 °C, though the same conclusion is that the $LiMn_2O_4$ nanowires material exhibits better cycling capacity at higher discharge C-rate. $LiMn_2O_4$ nano-wires were used as a new electrode material for the aqueous solution lithium-ion battery relying on their advantages. Although the battery (LiV_3O_8//$LiMn_2O_4$ nanowires) performance is measured at different C-rates, it is very strange that high C-rate brought stable capacity against cycles. Initial capacity looks to be nearly the same at the C-rates, thus this capacity degradation will not be due to the difference of lithium insertion depth into the nanowires. Precipitations formed on the electrode surface may indicate the instability of $LiMn_2O_4$ nanowires with large surface area in the tested aqueous solution. At that case, higher degradation properties at lower C-rate just might originate from the difference of immersion time of the samples in the aqueous electrolyte.

To our best knowledge that the electrode reaction of the aqueous solution lithium-ion battery is not simple and is composed of several reaction steps, such as a phase transition of the electrode active material, electron conduction and ion diffusion, and charge transfer reaction. Among these, this charge transfer reaction is rec-

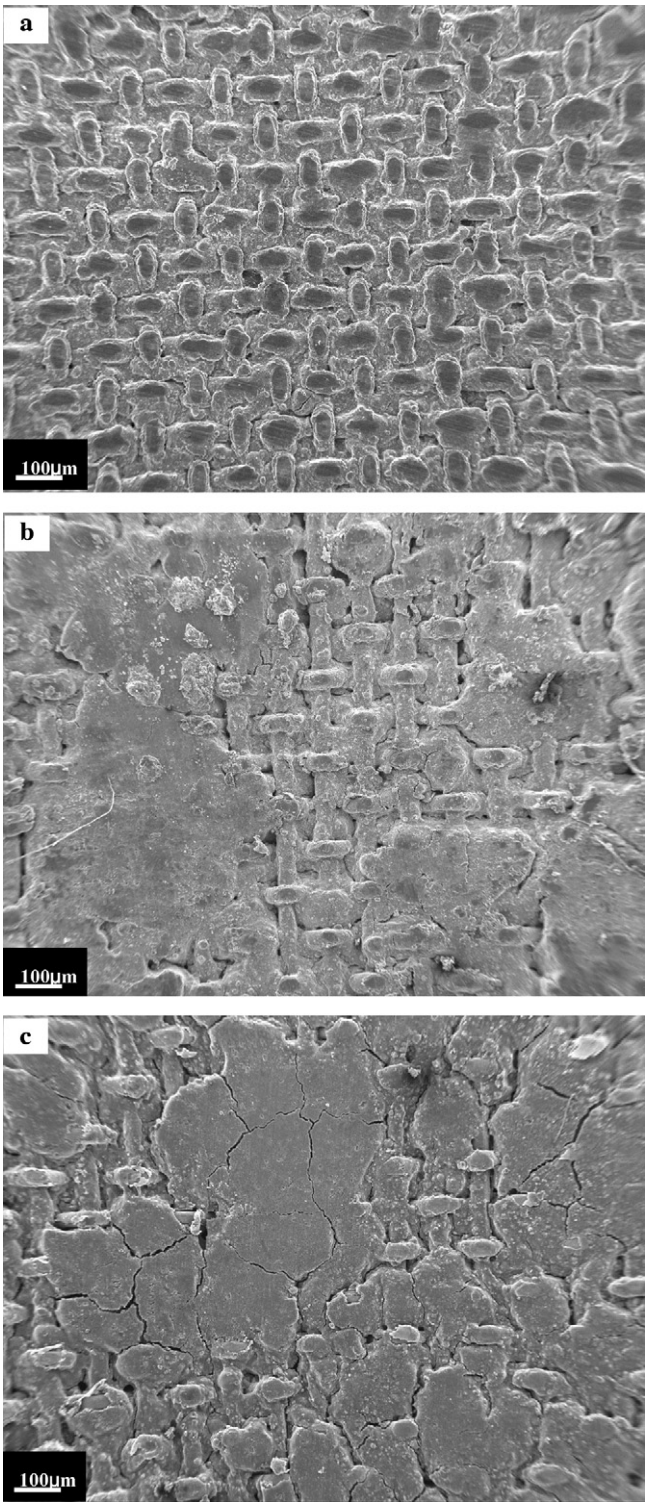

Fig. 7. SEM images of the ARLB electrode before and after 56, 130 cycels. (a) before initial discharge. (b) after 56 cycles. (c) after 130 cycles.

ognized as an interfacial lithium ion transfer reaction and not a general electron transfer reaction. Particularly, this charge transfer reaction rate is strongly related to the rate capability of the charge–discharge reaction. It is expected that a rate determining step for the charge transfer reaction will be a dissolution process of lithium ions at the intercalation site of the electrode active material. This activation energy must be mainly determined by the dissolution reaction [43]. And the interactions between the lithium ions and electrode surface of the active material during the dissolution process in the aqueous solution are underway.

Furthermore, to explore the reasons for capacity fading and directly analyses any changes in the morphology of the nanowires during cycling, the electrode fabricated from the cathode active materials of $LiMn_2O_4$ nanowires observed before and after 56, 130 cycles at 10C-rate with SEM. Fig. 7(a) is a SEM image showing the surface of the single crystalline $LiMn_2O_4$ nanowires electrode before cycle, where the integrity of electrode can be clearly observed. Then after 56 cycles, some plates aggregations are obviously seen on the surface of electrode displayed in Fig. 7(b). However, after 130 cycles, some cracks can be clearly observed on the surface of the electrode, where the integrity of the electrode is retained shown in Fig. 7(c). It may be deduced from those active materials detaching from the electrode due to $LiMn_2O_4$ nanowires volume change during charging/discharging. In addition, the irreversible variations of spinel cubic structure in the cycling existed for the $LiMn_2O_4$ nanowire material, and those variations can be speculated due to Jahn-Teller effect [35], which deduced nano structure lattice distortion, and manganese dissolution in the aqueous $LiNO_3$ electrolyte. Moreover, the investigations in this direction are under way.

4. Conclusions

The electrochemical performances of a new intercalate electrode material, $LiMn_2O_4$ single crystalline nanowires, in an aqueous $LiNO_3$ electrolyte is first studied by galvanostatic cycling. This ARLB is principally safe and environment friendly. It exhibits good cycling stability and especially it is beneficial to a high power lithium-ion battery due to its good electrochemical performance at the high C-rate. Therefore it appears great potential for applications in large-scale devices.

Acknowledgements

The authors acknowledge Shaan Xi Province Natural Science Fund (2010JM6018), Xi'an Applied Materials Innovation Fund (XA-AM-2008-16) and Xi'an Jiaotong University Inter-disciplinary Project Fund (0109-08140020).

References

[1] V.G. Kumar, J.S. Gnanaraj, S. Ben-David, D.M. Pickup, E.R.H. Van-Eck, A. Gedanken, D. Aurbach, Chem. Mater. 15 (2003) 4211.
[2] C.H. Jiang, S.X. Dou, H.K. Liu, M. Ichihara, H.S. Zhou, J. Power Sources 172 (2007) 410.
[3] T. Doi, T. Yahiro, S. Okada, J. Yamaki, Electrochim. Acta 53 (2008) 8064.
[4] M.C. Tucker, J.A. Reimer, E.J. Cairns, J. Electrochem. Soc. 149 (2002) A574.
[5] Y. Shin, A. Manthiram, Electrochem. Solid-State Lett. 5 (2002) A55.
[6] Y. Shin, A. Manthiram, J. Electrochem. Soc. 151 (2004) A204.
[7] C. Sigala, D. Guyomard, A. Verbaere, Y. Piffard, M. Tournoux, Solid State Ionics 81 (1995) 167.
[8] Y.P. Fu, Y.H. Su, C.H. Lin, Solid State Ionics 166 (2004) 137.
[9] I.B. Stojkovic, A. Hosseinmardi, D. Jugovic, M. Mitric, N.D. Cvjeticanin, Solid State Ionics 177 (2006) 847.
[10] N.D. Cvjeticanin, I.B. Stojkovic, M. Mitric, S.V. Mentus, J. Power Sources 174 (2007) 1117.
[11] M.S. Zhao, X.P. Song, Trans. Nonferrous Met. Soc. China 14 (2004) 811.
[12] M.S. Zhao, X.P. Song, J. Power Sources 164 (2007) 822.
[13] H.W. Ha, N.J. Yun, K. Kim, Electrochim. Acta 52 (2007) 3236.
[14] H. Sahan, H. Goktepe, S. Patat, A. Ulgen, Solid State Ionics 178 (2008) 1837.
[15] J.M. Amarilla, R.M. Rojas, F. Pico, L. Pascual, K. Petrov, D. Kovacheva, M.G. Lazarraga, I. Lejona, J.M. Rojo, J. Power Sources 174 (2007) 1212.
[16] L.F. Xiao, Y.Q. Zhao, Y.Y. Yang, Y.L. Cao, X.P. Ai, H.X. Yang, Electrochim. Acta 54 (2008) 545.
[17] S. Maa, K. Namb, W. Yoonc, S. Bak, X. Yang, B. Cho, K. Kim, Electrochem. Commun. 11 (2009) 1575.
[18] W. Li, W.R. Mckinnon, J.R. Dahn, J. Electrochem. Soc. 141 (1994) 2310.
[19] W. Li, J.R. Dahn, J. Electrochem. Soc. 142 (1995) 1742.
[20] W. Li, J.R. Dahn, D.S. Wainwright, Science 264 (1994) 1115.
[21] I.B. Stojkovic, N.D. Cvjeticanin, S.V. Mentus, Electrochem. Commun. 12 (2010) 371.

[22] R. Ruffo, C. Wessells, R.A. Huggins, Y. Cui, Electrochem. Commun. 11 (2009) 247.
[23] N. Li, C.J. Patrissi, G. Che, C.R. Martin, J. Electrochem. Soc. 147 (2000) 2044.
[24] G.J. Wang, Q.T. Qu, B. Wang, Y. Shi, S. Tian, Y. Wu, ChemPhysChem 9 (2008) 2299.
[25] L. Tian, A. Yuan, J. Power Sources 192 (2009) 693.
[26] M.S. Zhao, Q.Y. Zheng, F. Wang, W.M. Dai, X.P. Song, Electrochimi. Acta 56 (2011) 3781.
[27] J.Y. Luo, W.J. Cui, P. He, Y.Y. Xia, Nat. Chem. 2 (2010) 760.
[28] C.H. Mi, X.G. Zhang, H.L. Li, J. Electroanal. Chem. 602 (2007) 245.
[29] C. Cheng, Z.H. Li, X.Y. Zhan, Q.Z. Xiao, G.T. Lei, X.D. Zhou, Electrochimi. Acta 55 (2010) 4627.
[30] I.B. Stojkovic, N.D. Cvjeticanin, I. Pasti, M. Mitric, S.V. Mentus, Electrochem. Commun. 11 (2009) 1512.
[31] F. Wang, Y. Liu, C. Liu, Electrochim. Acta 55 (2010) 2662.
[32] G.J. Wang, Q.T. Qu, B. Wang, Y. Shi, S. Tian, Y.P. Wu, R. Holze, Electrochim. Acta 54 (2009) 1199.
[33] G.J. Wang, L.C. Yang, Q.T. Qu, B. Wang, Y.P. Wu, R. Holze, J. Solid State Electrochem. 14 (2010) 865.
[34] H. Castaneda, B. Tan, J. Saunders, Electrochimi. Acta 55 (2010) 4137.
[35] E. Hosono, T. Kudo, I. Honma, H. Matsuda, H. Zhou, Nano Lett. 9 (2009) 1045.
[36] M. Adachi, Y. Murata, J. Takao, J. Jiu, M. Sakamoto, F. Wang, J. Am. Chem. Soc. 126 (2004) 14943.
[37] D.N. Futaba, K. Hata, T. Yamada, T. Hiraoka, Y. Hayamizu, Y. Kakudate, O. Tanaike, H. Hatori, M. Yumura, S. Iijima, Nat. Mater. 5 (2006) 987.
[38] H.J. Fan, M. Knez, R. Scholz, K. Nielsch, E. Pippel, D. Hesse, M. Zacharias, U. Gosele, Nat. Mater. 5 (2006) 627.
[39] Y. Tian, D. Chen, X. Jiao, Y. Duan, Chem. Commun. (2007) 2072.
[40] L. Zhang, J.C. Yu, A.W. Xu, Q. Li, K.W. Kwong, L. Wu, Chem. Commun. (2003) 2910.
[41] D.K. Kim, P. Muralidharan, H. Lee, R. Ruffo, Y. Yang, C.K. Chan, H. Peng, R.A. Huggins, Y. Cui, Nano Lett. 8 (2008) 3948.
[42] H. Lee, P. Muralidharan, R. Ruffo, C.M. Mari, Y. Cui, D.K. Kim, Nano Lett. 10 (2010) 3852.
[43] N. Nakayama, I. Yamada, Y. Huang, T. Nozawa, Y. Iriyama, T. Abe, Z. Ogumi, Electrochim. Acta 54 (2009) 3428.